

# Cosmological constraints on the generalized holographic dark energy

Jianbo Lu,<sup>1,\*</sup> Yuting Wang,<sup>2</sup> Yabo Wu,<sup>1</sup> and Tianqiang Wang<sup>1</sup>

<sup>1</sup>*Department of Physics, Liaoning Normal University, Dalian 116029, P. R. China*

<sup>2</sup>*School of Physics and Optoelectronic Technology,  
Dalian University of Technology, Dalian, 116024, P. R. China*

We use the Markov Chain Monte Carlo method to investigate a global constraints on generalized holographic (GH) dark energy with flat and non-flat universe from the current observed data: the Union2 dataset of type supernovae Ia (SNIa), high-redshift Gamma-Ray Bursts (GRBs), the observational Hubble data (OHD), the cluster X-ray gas mass fraction, the baryon acoustic oscillation (BAO), and the cosmic microwave background (CMB) data. The most stringent constraints on GH model parameter are obtained. In addition, it is found that the equation of state for this generalized holographic dark energy can cross over the phantom boundary  $w_{de} = -1$ .

PACS numbers: 98.80.-k

Keywords: Generalized holographic dark energy; Combined constraints; Markov Chain Monte Carlo.

## I. Introduction

The late accelerating universe [1] is often interpreted by introducing a new component dubbed as dark energy (DE) with negative pressure in the standard cosmology. And a natural candidate of DE is positive tiny cosmological constant, though it suffers from both the fine tuning and cosmic coincidence problems. If DE is not a constant but a time variable one, the fine tuning and cosmic coincidence problems can be solved. So, lots of dynamical dark energy models were investigated in the past years [2]. Especially, the energy density given by basing the holographic principle are studied extensively [3]. According to the holographic principle it is required that the total energy for a system with size  $L$  should not exceed the mass of a black hole of the same size. The largest  $L$  allowed indicates an energy density  $\rho_\Lambda = 3c^2 M_p^2 L^{-2}$ , where  $c$  is a numerical constant and  $M_p$  is the reduced Planck Mass  $M_p^{-2} = 8\pi G$ . Applying this principle to cosmology, the UV cut-off is related to the vacuum energy, and IR cut-off is related to the large scale of the universe such as Hubble horizon, future event horizon, particle horizon, etc. And an accelerated universe can be gotten by taking the future event horizon as an IR cut-off, with existing a causality problem. Unfortunately, though the Hubble horizon is the most natural cosmological length scale, non-accelerated universe can be obtained [3] when this horizon is taken as the IR cut-off. So, how to obtain an accelerated expansion by using the Hubble horizon as the IR cut-off is interesting.

In addition, on the basis of holographic principle Ref. [4] take the Ricci scalar as the IR cut-off and obtain a new form of energy density,  $\rho_R = 3c^2 M_p^2 (\dot{H} + 2H^2 + k/a^2) \propto R$ , dubbed as Ricci dark energy. For this model it avoid the causality problem and solve the coincidence problem [4]. And in Ref. [5] it is found that the Ricci dark energy has

---

\*Electronic address: lvjianbo819@163.com

relation with the causal connection scale  $R^{-2} = \text{Max}(\dot{H} + 2H^2, -\dot{H})$  for a flat universe. Also, it is shown that for these two cases only taking  $R^{-2} = \dot{H} + 2H^2$  as the IR cut-off, the obtained model is consistent with the current cosmic observations when the dark energy is looked as an independently conserved component  $\dot{\rho}_{de} + 3H(\rho_{de} + P_{de}) = 0$  [5]. And as indicated in Ref. [6],  $H^2$  or  $\dot{H}$  alone can not provide an late accelerated universe that is consistent with the current cosmic observations. So, the generalized holographic (or Ricci) dark energy model, i.e. a form of their combination is investigated in Ref. [6]. In this paper we applying the current observed data to constrain the generalized holographic (GH) dark energy model by using the Markov Chain Monte Carlo (MCMC) method.

## II. Basic equations for generalized holographic dark energy

In a Friedmann-Robertson-Walker universe, when the Hubble horizon and Ricci scalar are taken as the IR cut-off, the holographic dark energy and Ricci dark energy are written as,  $\rho_h = 3c^2 M_p^2 H^2$  and  $\rho_R = 3c^2 M_p^2 R$ , respectively. And in order to compare the holographic and the Ricci dark energy, and to obtain an accelerated universe by using the Hubble horizon as the IR cut-off, in Ref. [6] a generalized version of holographic dark energy are constructed as,

$$\rho_{GH} = 3c^2 M_p^2 f\left(\frac{R}{H^2}\right) H^2, \quad (1)$$

where  $f(x)$  is a function of the dimensionless variable  $x = R/H^2$ , and it is interesting to write the function as [6],

$$f\left(\frac{R}{H^2}\right) = 1 - \epsilon\left(1 - \frac{R}{H^2}\right), \quad (2)$$

where  $\epsilon$  is parameter. For the generalized form of energy density, when  $\epsilon = 0$  or  $\epsilon = 1$ , it becomes holographic or Ricci dark energy density, respectively. Thus for this generalized model, the dark energy density is expressed as

$$\begin{aligned} \rho_{GH} &= 3c^2 M_p^2 \left[1 - \epsilon\left(1 - \frac{R}{H^2}\right)\right] H^2 \\ &= 3c^2 M_p^2 \left[1 - \epsilon\left(1 - \frac{\dot{H} + 2H^2}{H^2}\right)\right] H^2 \\ &= 3c^2 M_p^2 \left[1 + \epsilon - \epsilon(1+z) \frac{1}{H} \frac{dH}{dz}\right] H^2. \end{aligned} \quad (3)$$

And its dimensionless dark energy density is described,

$$\begin{aligned} \Omega_{GH} &\equiv \frac{\rho_{GH}}{3M_p^2 H^2} \\ &= c^2 \left[1 + \epsilon - \epsilon(1+z) \frac{d \ln H}{dz}\right]. \end{aligned} \quad (4)$$

For the generalized holographic dark energy model, the corresponding Friedmann equation can be written as,

$$H^2 = H_0^2 \left[ \frac{2(\Omega_{0m}(1+z)^3 + \Omega_r(1+z)^4 + \Omega_k(1+z)^2)}{2 + c^2(\epsilon - 2)} + \left(1 - \frac{2(\Omega_{0m} + \Omega_r + \Omega_k)}{2 + c^2(\epsilon - 2)}\right) (1+z)^{2 - \frac{2}{c^2\epsilon} + \frac{2}{\epsilon}} \right], \quad (5)$$

where  $\Omega_{0m}$ ,  $\Omega_r$  and  $\Omega_k$  respectively denotes the current value of dimensionless matter, photon and curvature density, here  $\Omega_{0m}$  include baryon matter  $\Omega_b$  and cold dark matter  $\Omega_c$ ,  $\Omega_{0m} = \Omega_b + \Omega_c$ . Furthermore, for the deceleration parameter  $q(z)$  and the geometrical diagnostic quantity  $Om(z)$  [7], they can be expressed by the Hubble parameter as,

$$q = -\frac{\ddot{a}}{aH^2} = -1 + (1+z) \frac{1}{H} \frac{dH}{dz}, \quad (6)$$

$$Om(z) \equiv \frac{E^2(z) - 1}{x^3 - 1}, \quad x = 1 + z = \frac{1}{a}, \quad E(z) = \frac{H(z)}{H_0}. \quad (7)$$

And the equation of state (EOS) of generalized holographic dark energy  $w_{GH}$  can be derived as,

$$w_{GH} = -1 + \frac{(1+z)}{3} \frac{1}{\rho_{GH}} \frac{d\rho_{GH}}{dz}, \quad (8)$$

according to the conservation equation with no interactions between two dark components  $\dot{\rho}_{GH} + 3H(1+w_{GH})\rho_{GH} = 0$ .

### III. The current observed data and cosmological constraint methods

In this part we introduce the cosmological constraint methods and the current observed data used in this paper. Concretely, it includes 557 Union2 dataset of type supernovae Ia (SNIa) [8], 59 high-redshift Gamma-Ray Bursts (GRBs) data [9], observational Hubble data (OHD) [10], X-ray gas mass fraction in cluster [11], baryon acoustic oscillation (BAO) [12], and cosmic microwave background (CMB) data [13].

#### A. Type Ia supernovae

For SNIa observations, we use the SNIa Union2 dataset that includes 557 SNIa [8]. Following [14, 15], one can obtain the corresponding constraints by fitting the distance modulus  $\mu(z)$ ,

$$\mu_{th}(z) = 5 \log_{10}[D_L(z)] + \mu_0. \quad (9)$$

In this expression  $D_L(z) = H_0 d_L(z)/c$  is the Hubble-free luminosity distance, with  $H_0$  being the Hubble constant described by the re-normalized quantity  $h$  as  $H_0 = 100h \text{ km s}^{-1} \text{ Mpc}^{-1}$ , and

$$d_L(z) = \frac{c(1+z)}{\sqrt{|\Omega_k|}} \text{sinn}[\sqrt{|\Omega_k|} \int_0^z \frac{dz'}{H(z')}],$$

$$\mu_0 = 5 \log_{10}\left(\frac{H_0^{-1}}{\text{Mpc}}\right) + 25 = 42.38 - 5 \log_{10} h,$$

where  $\text{sinn}(\sqrt{|\Omega_k|}x)$  respectively denotes  $\sin(\sqrt{|\Omega_k|}x)$ ,  $\sqrt{|\Omega_k|}x$ , and  $\sinh(\sqrt{|\Omega_k|}x)$  for  $\Omega_k < 0$ ,  $\Omega_k = 0$  and  $\Omega_k > 0$ . Additionally, the observed distance moduli  $\mu_{obs}(z_i)$  of SNIa at  $z_i$  is

$$\mu_{obs}(z_i) = m_{obs}(z_i) - M, \quad (10)$$

where  $m$  and  $M$  are apparent magnitude and absolute magnitude of SNIa.

For using SNIa data, theoretical model parameters  $p_s$  can be determined by a likelihood analysis, based on the calculation of

$$\begin{aligned} \chi^2(p_s, M') &\equiv \sum_{SNIa} \frac{\{\mu_{obs}(z_i) - \mu_{th}(p_s, z_i)\}^2}{\sigma_i^2} \\ &= \sum_{SNIa} \frac{\{5 \log_{10}[D_L(p_s, z_i)] - m_{obs}(z_i) + M'\}^2}{\sigma_i^2}, \end{aligned} \quad (11)$$

where  $M' \equiv \mu_0 + M$  is a nuisance parameter which includes the absolute magnitude and the parameter  $h$ . The nuisance parameter  $M'$  can be marginalized over analytically [16] as

$$\bar{\chi}^2(p_s) = -2 \ln \int_{-\infty}^{+\infty} \exp \left[ -\frac{1}{2} \chi^2(p_s, M') \right] dM',$$

resulting to

$$\bar{\chi}^2 = A - \frac{B^2}{C} + \ln\left(\frac{C}{2\pi}\right), \quad (12)$$

with

$$\begin{aligned} A &= \sum_{SNIa} \frac{\{5 \log_{10}[D_L(p_s, z_i)] - m_{obs}(z_i)\}^2}{\sigma_i^2}, \\ B &= \sum_{SNIa} \frac{5 \log_{10}[D_L(p_s, z_i)] - m_{obs}(z_i)}{\sigma_i^2}, \\ C &= \sum_{SNIa} \frac{1}{\sigma_i^2}. \end{aligned}$$

Relation (11) has a minimum at the nuisance parameter value  $M' = B/C$ , which contains information of the values of  $h$  and  $M$ . Considering that the expression

$$\chi_{SNIa}^2(p_s) = A - (B^2/C), \quad (13)$$

is only different from Eq. (12) with a constant term  $\ln(C/2\pi)$ , it is often used in the likelihood analysis [14, 16].

### B. High-redshift Gamma-Ray Bursts data

The GRBs data can be observed at higher redshift than SNIa. The currently observed redshift range of GRBs is at  $0.1 \lesssim z \lesssim 9$ . Therefore, the GRBs data can be viewed as an excellent complement to SNIa data and would provide more information at high redshift. When several empirical relations of the GRBs are proposed, these indicators have motivated the authors make use of the GRBs as cosmological standard candles at high redshift. However, the fact that there are not sufficient low redshift GRBs leads that the calibration of GRB relations is dependent on the cosmological model, namely, the circularity problem. One of methods to solve the circularity problem is the calibration of GRB relations are performed by the use of a sample of SNIa at low redshift in the cosmology-independent way [17]. Here, the GRBs data we used consists of 59 GRB samples with a redshift range of  $1.4 \lesssim z \lesssim 9$  obtained in [9]. These 59 GRBs are calibrated by utilizing the newly released 557 Uion2 SNIa and the isotropic energy-peak spectral energy ( $E_{iso} - E_{p,i}$ ) relation (i.e. Amati relation) [18].

The  $\chi_{GRBs}^2$  takes the same form as  $\chi_{SNIa}^2$

$$\chi_{GRBs}^2(p_s, \mu_0) = \sum_{i=1}^{59} \frac{[\mu_{obs}(z_i) - \mu_{th}(z_i; p_s, \mu_0)]^2}{\sigma_i^2}. \quad (14)$$

The same method are used to deal with the nuisance parameter  $\mu_0$  as shown in the description of  $\chi_{SNIa}^2$  above.

### C. Observational Hubble data

The observational Hubble data [19] are given by basing the differential ages of the galaxies. In [20], Jimenez *et al.* obtain an independent estimate for Hubble parameter, and use it to constrain the cosmological models. The Hubble parameter as a function of redshift  $z$  can be written in the form of

$$H(z) = -\frac{1}{1+z} \frac{dz}{dt}. \quad (15)$$

So, once  $dz/dt$  is known,  $H(z)$  is obtained directly. By using the differential ages of passively-evolving galaxies, Refs. [10, 21, 22] obtain twelve values of  $H(z)$  at different redshift (redshift interval  $0 \lesssim z \lesssim 1.8$ ), as listed in Table I. In

$z$	0	0.1	0.17	0.27	0.4	0.48	0.88	0.9	1.30	1.43	1.53	1.75
$H(z)$ (km s <sup>-1</sup> Mpc <sup>-1</sup> )	74.2	69	83	77	95	97	90	117	168	177	140	202
$1\sigma$ uncertainty	$\pm 3.6$	$\pm 12$	$\pm 8$	$\pm 14$	$\pm 17$	$\pm 60$	$\pm 40$	$\pm 23$	$\pm 17$	$\pm 18$	$\pm 14$	$\pm 40$

TABLE I: The observational  $H(z)$  data [21, 22].

addition, in [23] the authors take the BAO scale as a standard ruler in the radial direction, and obtain three more additional data:  $H(z = 0.24) = 79.69 \pm 2.32$ ,  $H(z = 0.34) = 83.8 \pm 2.96$ , and  $H(z = 0.43) = 86.45 \pm 3.27$ .

The values of model parameters can be determined according to the observational Hubble data by minimizing [24]

$$\chi_{OHD}^2(H_0, p_s) = \sum_{i=1}^{15} \frac{[H_{th}(H_0, p_s; z_i) - H_{obs}(z_i)]^2}{\sigma^2(z_i)}, \quad (16)$$

where  $H_{th}$  is the predicted value of the Hubble parameter,  $H_{obs}$  is the observed value,  $\sigma(z_i)$  is the standard deviation measurement uncertainty, and the summation is over the 15 observational Hubble data points at redshifts  $z_i$ .

#### D. The X-ray gas mass fraction

The X-ray gas mass fraction,  $f_{gas}$ , is defined as the ratio of the X-ray gas mass to the total mass of a cluster, which is approximately independent on the redshift for the hot ( $kT \gtrsim 5keV$ ), dynamically relaxed clusters at the radii larger than the innermost core  $r_{2500}$ . As investigated in [11], the  $\Lambda$ CDM model is much favored and is chosen as the referenced cosmology. The model fitted to the referenced  $\Lambda$ CDM data is presented as [11]

$$f_{gas}^{\Lambda CDM}(z) = \frac{KA\gamma b(z)}{1+s(z)} \left( \frac{\Omega_b}{\Omega_{0m}} \right) \left[ \frac{D_A^{\Lambda CDM}(z)}{D_A(z)} \right]^{1.5}, \quad (17)$$

where  $D_A^{\Lambda CDM}(z)$  and  $D_A(z)$  denote respectively the proper angular diameter distance in the  $\Lambda$ CDM cosmology and the current constraint model.  $A$  is the angular correction factor, which is caused by the change in angle for the current test model  $\theta_{2500}$  in comparison with that of the reference cosmology  $\theta_{2500}^{\Lambda CDM}$ :

$$A = \left( \frac{\theta_{2500}^{\Lambda CDM}}{\theta_{2500}} \right)^\eta \approx \left( \frac{H(z)D_A(z)}{[H(z)D_A(z)]^{\Lambda CDM}} \right)^\eta, \quad (18)$$

here, the index  $\eta$  is the slope of the  $f_{gas}(r/r_{2500})$  data within the radius  $r_{2500}$ , with the best-fit average value  $\eta = 0.214 \pm 0.022$  [11]. And the proper (not comoving) angular diameter distance is given by

$$D_A(z) = \frac{c}{(1+z)\sqrt{|\Omega_k|}} \text{sinn}[\sqrt{|\Omega_k|} \int_0^z \frac{dz'}{H(z')}] . \quad (19)$$

It is clear that this quantity is related with  $d_L(z)$  by

$$D_A(z) = \frac{d_L(z)}{(1+z)^2}.$$

In equation (17), the parameter  $\gamma$  denotes permissible departures from the assumption of hydrostatic equilibrium, due to non-thermal pressure support; the bias factor  $b(z) = b_0(1 + \alpha_b z)$  accounts for uncertainties in the cluster depletion

factor;  $s(z) = s_0(1 + \alpha_s z)$  accounts for uncertainties of the baryonic mass fraction in stars and a Gaussian prior for  $s_0$  is employed, with  $s_0 = (0.16 \pm 0.05)h_{70}^{0.5}$  [11]; the factor  $K$  is used to describe the combined effects of the residual uncertainties, such as the instrumental calibration and certain X-ray modelling issues, and a Gaussian prior for the 'calibration' factor is considered by  $K = 1.0 \pm 0.1$  [11].

Following the method in Ref. [11, 25] and adopting the updated 42 observational  $f_{gas}$  data in Ref. [11], the values of model parameters for the X-ray gas mass fraction analysis are determined by minimizing,

$$\chi_{CBF}^2 = \sum_i^N \frac{[f_{gas}^{\Lambda CDM}(z_i) - f_{gas}(z_i)]^2}{\sigma_{f_{gas}}^2(z_i)} + \frac{(s_0 - 0.16)^2}{0.0016^2} + \frac{(K - 1.0)^2}{0.01^2} + \frac{(\eta - 0.214)^2}{0.022^2}, \quad (20)$$

where  $\sigma_{f_{gas}}(z_i)$  is the statistical uncertainties (Table 3 of [11]). As pointed out in [11], the acquiescent systematic uncertainties have been considered according to the parameters i.e.  $\eta$ ,  $b(z)$ ,  $s(z)$  and  $K$ .

### E. Baryon acoustic oscillation

The baryon acoustic oscillations are detected in the clustering of the combined 2dFGRS and SDSS main galaxy samples, which measure the distance-redshift relation at  $z_{BAO} = 0.2$  and  $z_{BAO} = 0.35$ . The observed scale of the BAO calculated from these samples, are analyzed using estimates of the correlated errors to constrain the form of the distance measure  $D_V(z)$  [12, 26]

$$D_V(z) = [(1+z)^2 D_A^2(z) \frac{cz}{H(z; p_s)}]^{1/3} = H_0 \left[ \frac{z}{E(z; p_s)} \left( \int_0^z \frac{dz'}{E(z'; p_s)} \right)^2 \right]^{1/3}. \quad (21)$$

In this expression  $E(z; p_s) = H(z; p_s)/H_0$ . The peak positions of the BAO depend on the ratio of  $D_V(z)$  to the sound horizon size at the drag epoch (where baryons were released from photons)  $z_d$ , which can be obtained by using a fitting formula

$$z_d = \frac{1291(\Omega_{0m}h^2)^{-0.419}}{1 + 0.659(\Omega_{0m}h^2)^{0.828}} [1 + b_1(\Omega_b h^2)^{b_2}], \quad (22)$$

with

$$b_1 = 0.313(\Omega_{0m}h^2)^{-0.419} [1 + 0.607(\Omega_{0m}h^2)^{0.674}], \quad (23)$$

$$b_2 = 0.238(\Omega_{0m}h^2)^{0.223}. \quad (24)$$

In this paper, we use the data of  $r_s(z_d)/D_V(z)$  extracted from the Sloan Digital Sky Survey (SDSS) and the Two Degree Field Galaxy Redshift Survey (2dFGRS) [26], which are listed in Table II, where  $r_s(z)$  is the comoving sound horizon size

$$\begin{aligned} r_s(z) &= c \int_0^t \frac{c_s dt}{a} = c \int_0^a \frac{c_s da}{a^2 H} = c \int_z^\infty dz \frac{c_s}{H(z)} \\ &= \frac{c}{\sqrt{3}} \int_0^{1/(1+z)} \frac{da}{a^2 H(a) \sqrt{1 + (3\Omega_b/(4\Omega_\gamma)a)}}, \end{aligned} \quad (25)$$

where  $c_s$  is the sound speed of the photon–baryon fluid

$$c_s^{-2} = 3 + \frac{4}{3} \times \frac{\rho_b(z)}{\rho_\gamma(z)} = 3 + \frac{4}{3} \times \left( \frac{\Omega_b}{\Omega_\gamma} \right) a. \quad (26)$$

$z$	$r_s(z_d)/D_V(z)$
0.2	$0.1905 \pm 0.0061$
0.35	$0.1097 \pm 0.0036$

TABLE II: The observational  $r_s(z_d)/D_V(z)$  data [12].

Using the data of BAO in Table II and the inverse covariance matrix  $V^{-1}$  in [12]:

$$V^{-1} = \begin{pmatrix} 30124.1 & -17226.9 \\ -17226.9 & 86976.6 \end{pmatrix}, \quad (27)$$

the  $\chi_{BAO}^2(p_s)$  is given as

$$\chi_{BAO}^2(p_s) = X^t V^{-1} X, \quad (28)$$

where  $X$  is a column vector formed from the values of theory minus the corresponding observational data, with

$$X = \begin{pmatrix} \frac{r_s(z_d)}{D_V(0.2)} - 0.1905 \\ \frac{r_s(z_d)}{D_V(0.35)} - 0.1097 \end{pmatrix}, \quad (29)$$

and  $X^t$  denotes its transpose.

## F. Cosmic microwave background

The CMB shift parameter  $R$  is provided by

$$R = \sqrt{\Omega_{0m} H_0^2} (1 + z_*) D_A(z_*) / c = \sqrt{\Omega_{0m}} \int_0^{z_*} \frac{H_0 dz'}{H(z'; p_s)}, \quad (30)$$

here, the redshift  $z_*$  (the decoupling epoch of photons) is obtained using the fitting function

$$z_* = 1048 [1 + 0.00124(\Omega_b h^2)^{-0.738}] [1 + g_1(\Omega_{0m} h^2)^{g_2}],$$

where the functions  $g_1$  and  $g_2$  read

$$\begin{aligned} g_1 &= 0.0783(\Omega_b h^2)^{-0.238} (1 + 39.5(\Omega_b h^2)^{0.763})^{-1}, \\ g_2 &= 0.560 (1 + 21.1(\Omega_b h^2)^{1.81})^{-1}. \end{aligned}$$

In addition, the acoustic scale is related to a distance ratio,  $D_A(z)/r_s(z)$ , and at decoupling epoch it is defined as

$$l_A \equiv (1 + z_*) \frac{\pi D_A(z_*)}{r_s(z_*)}, \quad (31)$$

where Eq.(31) arises a factor  $1 + z_*$ , because  $D_A(z)$  is the proper angular diameter distance, whereas  $r_s(z_*)$  is the comoving sound horizon. Using the data of  $l_A, R, z_*$  in [13] and their covariance matrix of  $[l_A(z_*), R(z_*), z_*]$  (please see table III and IV), we can calculate the likelihood  $L$  as  $\chi_{CMB}^2 = -2 \ln L$ :

$$\chi_{CMB}^2 = \Delta d_i [Cov^{-1}(d_i, d_j) [\Delta d_i]^t], \quad (32)$$

where  $\Delta d_i = d_i - d_i^{data}$  is a row vector, and  $d_i = (l_A, R, z_*)$ .

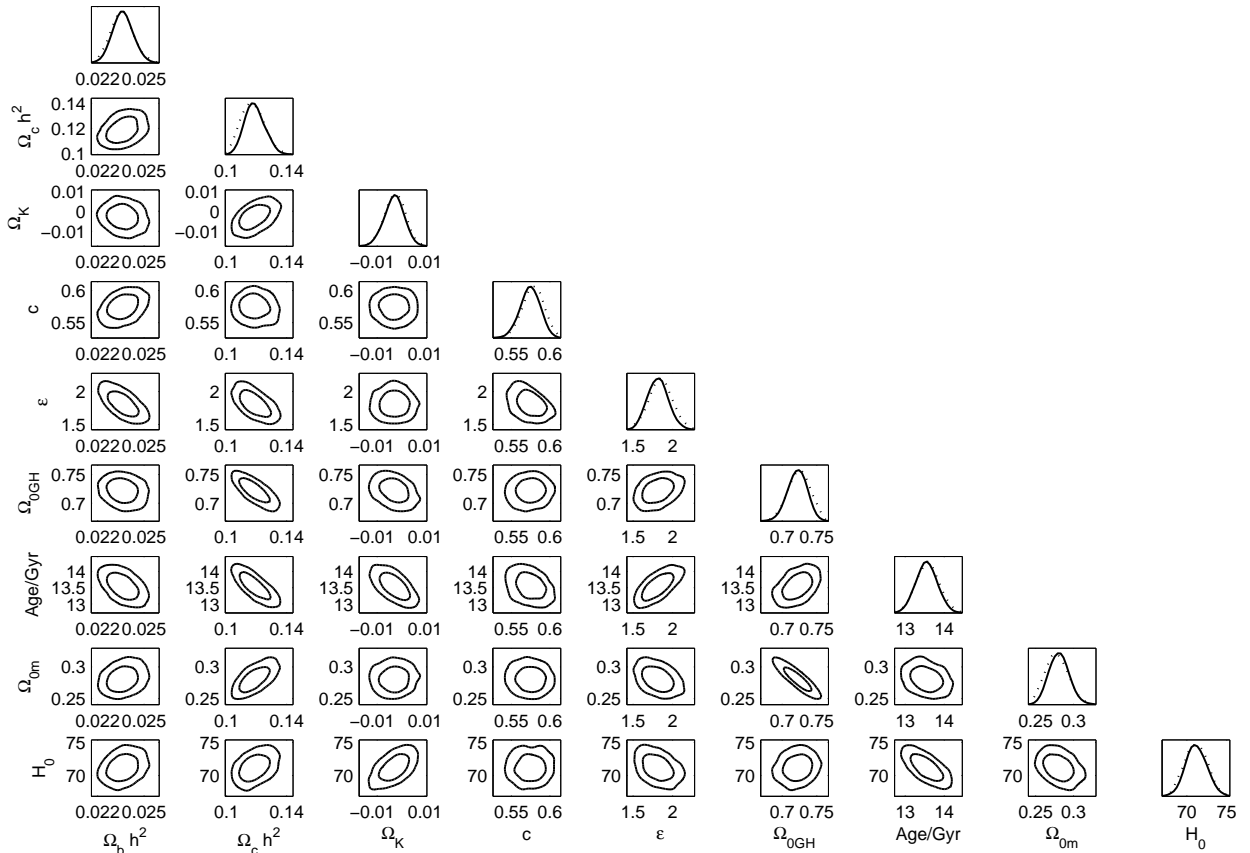


FIG. 1: The 2-D contours with  $1\sigma, 2\sigma$  confidence levels and 1-D distribution of model parameters in the non-flat GH model. Solid lines are mean likelihoods of samples, and dotted lines are marginalized probabilities for 1D distribution.

	7-year maximum likelihood	error, $\sigma$
$l_A(z_*)$	302.09	0.76
$R(z_*)$	1.725	0.018
$z_*$	1091.3	0.91

TABLE III: The values of  $l_A(z_*)$ ,  $R(z_*)$ , and  $z_*$  from 7-year WMAP data.

#### IV. Observed constraints on generalized holographic DE model by using MCMC method

Next we apply the Markov Chain Monte Carlo method to investigate a global constraint on above generalized holographic dark energy model. The MCMC source code can be found in the CosmoMC package [27] and the modified CosmoMC package [11, 28, 29] (this package is about the constraint code of X-ray cluster gas mass fraction). To get the converged results, in MCMC calculation we test the convergence of the chains by taking  $R - 1$  to be less



	$l_A(z_*)$	$R(z_*)$	$z_*$
$l_A(z_*)$	2.305	29.698	-1.333
$R(z_*)$		6825.270	-113.180
$z_*$			3.414

TABLE IV: The inverse covariance matrix of  $l_A(z_*)$ ,  $R(z_*)$ , and  $z_*$  from 7-year WMAP data.

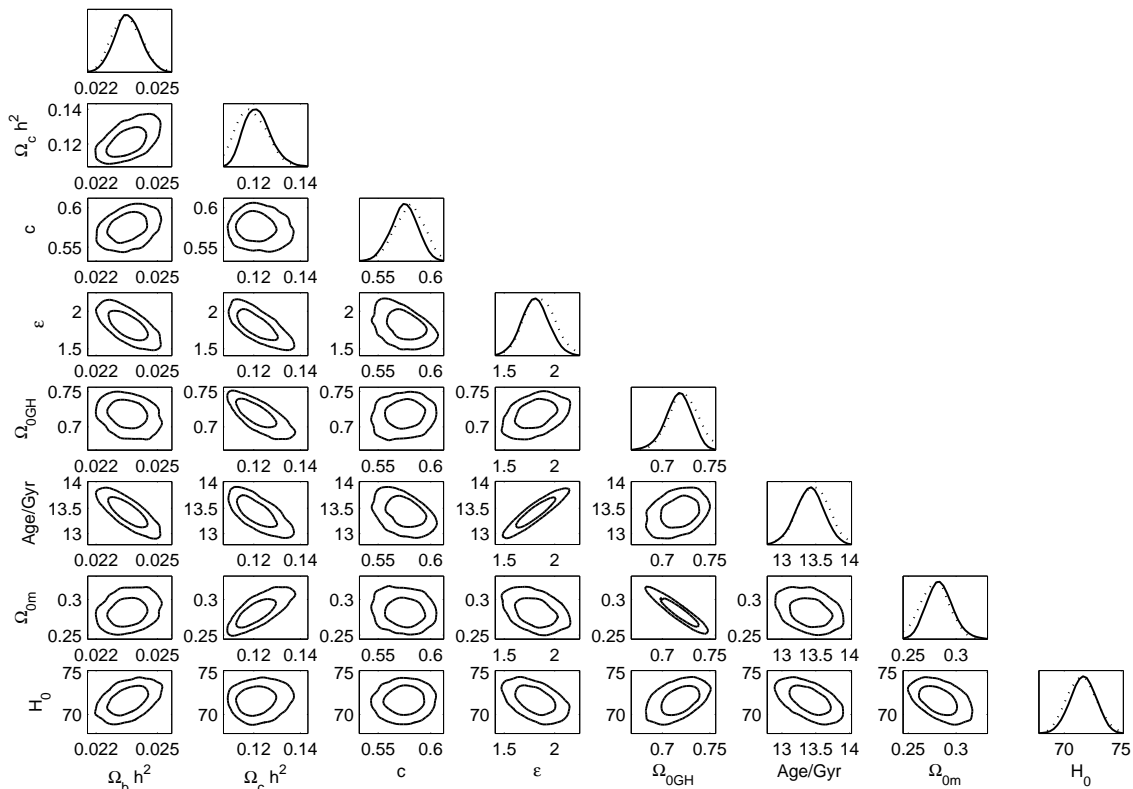


FIG. 2: The 2-D contours with  $1\sigma$ ,  $2\sigma$  confidence levels and 1-D distribution of model parameters in the flat GH model. Solid lines are mean likelihoods of samples, and dotted lines are marginalized probabilities for 1D distribution.

than 0.03. The total  $\chi^2$  is expressed as,

$$\chi_{total}^2(p_s) = \chi_{SNIa}^2 + \chi_{GRBs}^2 + \chi_{OHD}^2 + \chi_{CBF}^2 + \chi_{BAO}^2 + \chi_{CMB}^2, \quad (33)$$

with the parameter vector reading

$$p_s = \{\Omega_b h^2, \Omega_c h^2, \Omega_k, \epsilon, c\}. \quad (34)$$

Here the expression of  $\chi^2$  for each observation corresponds to Eqs.(13), (14), (16), (20), (28) and (32). Based on the basic cosmological parameters  $p_s$  we can also obtain the derived parameters  $\Omega_{0m} = \Omega_b + \Omega_c$ ,  $\Omega_{0GH} = 1 - \Omega_{0m} - \Omega_k$ , and the Hubble constant  $H_0 = 100h \text{ km}\cdot\text{s}^{-1}\cdot\text{Mpc}^{-1}$ . Using the currently observed data with the  $\chi_{total}^2$  in Eq. (33), Figs.

1 and 2 plot the 2-D contours with  $1\sigma, 2\sigma$  confidence levels and 1-D distribution of model parameters in the flat and non-flat generalized holographic dark energy model. Solid lines are mean likelihoods of samples, and dotted lines are marginalized probabilities for 1D distribution. Table V lists the MCMC calculation results for the constraint on model parameters. It includes the means, standard deviations with the marginalized limits for the model parameters, and the values for the best-fit sample, and projections of the n-dimensional  $1\sigma$  and  $2\sigma$  confidence regions. The n-D limits give some idea of the range of the posterior, and are much more conservative than the marginalized limits [27]. From the table V it can be seen that for the non-flat universe, the best fit results are given as  $\Omega_k = -0.0047^{+0.0132+0.0159}_{-0.0089-0.0120}$ ,  $c = 0.576^{+0.034+0.037}_{-0.036-0.053}$ ,  $\epsilon = 1.849^{+0.347+0.461}_{-0.380-0.442}$ ,  $\Omega_{0m} = 0.280^{+0.036+0.047}_{-0.032-0.040}$  (it has a smaller value of  $\Omega_{0m}$  relative to the case of constraints on the Ricci dark energy model [30, 31]), with  $\chi^2_{min} = 619.314$ . And for this case, it predicts the age of universe  $t_{age} = 13.711^{+0.709+0.924}_{-0.859-0.978}$ (Gyr). Furthermore, comparing the Ref. [6] one can see that for the generalized holographic dark energy the more stringent constraint on model parameters at  $2\sigma$  confidence level are given in this paper by using the more observational data, and it tends to have a smaller value of dimensionless matter density  $\Omega_{0m}$  and a bigger value of model parameter  $\epsilon$ .

	Non-flat	Non-flat	Flat	Flat
Parameters	Best fit values	Means	Best fit values	Means
$\Omega_b h^2$	$0.0233^{+0.0023+0.0027}_{-0.0016-0.0016}$	$0.0236^{+0.0006+0.0013}_{-0.0006-0.0012}$	$0.0236^{+0.0018+0.0022}_{-0.0017-0.0022}$	$0.0236^{+0.0006+0.0012}_{-0.0007-0.0012}$
$\Omega_c h^2$	$0.1150^{+0.0220+0.0290}_{-0.0160-0.0160}$	$0.1188^{+0.0067+0.0133}_{-0.0065-0.0120}$	$0.1178^{+0.0195+0.0241}_{-0.0105-0.0121}$	$0.1217^{+0.0055+0.0126}_{-0.0056-0.0097}$
$\Omega_k$	$-0.0047^{+0.0132+0.0159}_{-0.0089-0.0120}$	$-0.0029^{+0.0040+0.0077}_{-0.0040-0.0168}$	—	—
$c$	$0.576^{+0.034+0.037}_{-0.036-0.053}$	$0.574^{+0.013+0.024}_{-0.012-0.026}$	$0.586^{+0.023+0.027}_{-0.043-0.052}$	$0.575^{+0.012+0.023}_{-0.013-0.025}$
$\epsilon$	$1.849^{+0.347+0.461}_{-0.380-0.442}$	$1.815^{+0.126+0.262}_{-0.129-0.237}$	$1.843^{+0.392+0.461}_{-0.347-0.429}$	$1.808^{+0.130+0.262}_{-0.129-0.255}$
$\Omega_{0m}$	$0.280^{+0.036+0.047}_{-0.032-0.040}$	$0.281^{+0.013+0.026}_{-0.013-0.024}$	$0.279^{+0.034+0.051}_{-0.035-0.037}$	$0.283^{+0.013+0.029}_{-0.013-0.024}$
$\Omega_{0GH}$	$0.725^{+0.035+0.041}_{-0.044-0.055}$	$0.722^{+0.013+0.025}_{-0.014-0.028}$	$0.721^{+0.035+0.037}_{-0.034-0.051}$	$0.717^{+0.013+0.024}_{-0.013-0.029}$
$H_0$	$70.361^{+4.710+5.143}_{-2.611-3.651}$	$71.181^{+1.313+2.627}_{-1.274-2.490}$	$71.170^{+3.514+3.939}_{-2.369-3.347}$	$71.656^{+1.102+2.056}_{-1.095-2.151}$
$t_{age}$ (Gyr)	$13.711^{+0.709+0.924}_{-0.859-0.978}$	$13.549^{+0.263+0.524}_{-0.267-0.515}$	$13.462^{+0.565+0.584}_{-0.589-0.747}$	$13.413^{+0.198+0.381}_{-0.200-0.402}$

TABLE V: For the flat and non-flat universe, the best fit model parameters with their limits from the extremal values of the n-dimensional distribution (recommended); and the means with the marginalized limits for the model parameters, from MCMC calculation by using SNIa Union2, GRBs, OHD, CBF, BAO, and CMB data.

	$z_T$	$q_0$	$Om_0$	$w_{0GH}$
Non-flat	$0.706^{+0.039}_{-0.036}$	$-0.639^{+0.042}_{-0.047}$	$0.241^{+0.047}_{-0.047}$	$-1.051^{+0.048}_{-0.048}$
Flat	$0.705^{+0.038}_{-0.034}$	$-0.598^{+0.041}_{-0.042}$	$0.268^{+0.043}_{-0.043}$	$-1.015^{+0.045}_{-0.045}$

TABLE VI: The best fit values of transition redshift, current values of deceleration parameter,  $Om$  parameter, and EOS of generalized holographic dark energy with their confidence levels for flat and non-flat universe.

In addition, according to the calculation of the covariance matrix and the best fit values of model parameters, the best fit evolutions of deceleration parameter  $q(z)$ , geometrical quantity  $Om(z)$  and EOS of dark energy  $w_{GH}(z)$  with their confidence level (shadow region) are plotted in Figs. 3 and 4. From the figures we can see that a current accelerated universe is obtained, and the equation of state for this generalized model can cross over the boundary of cosmological constant  $w_\Lambda(z) = -1$ . And for this generalized dark energy model, the predicted values of some

	$\eta$	$\gamma$	$K$	$b_0$	$\alpha_b$	$s_0$	$\alpha_s$
Non-flat	0.212	1.081	0.998	0.732	-0.092	0.174	-0.055
Flat	0.208	1.025	0.958	0.783	-0.086	0.156	0.020

TABLE VII: The best fit values of parameters in  $f_{gas}$  analysis method for flat and non-flat universe.

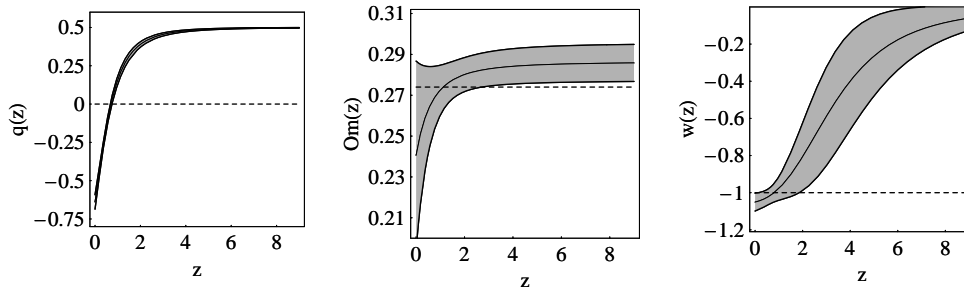


FIG. 3: The evolution of  $q(z)$ ,  $Om(z)$  and  $w_{de}(z)$  for non-flat generalized holographic model.

cosmological parameters with flat and non-flat universe according to above combined constraints are listed in table VI. From this table, it can be found that the current values of the deceleration parameter and the EOS of GH model are,  $q_0 = -0.639_{-0.047}^{+0.042}$ ,  $w_{0GH} = -1.051_{-0.048}^{+0.048}$  for non-flat universe, and  $q_0 = -0.598_{-0.042}^{+0.041}$ ,  $w_{0GH} = -1.015_{-0.045}^{+0.045}$  for flat universe. At last as an appendant, in table VII we also show the best fit values of several parameters in  $f_{gas}$  analysis method.

By the way, in appendix we also list the constraint results on another generalized model in Ref. [6], i.e. generalized Ricci DE by using the MCMC method and above observed data.

## V. Conclusions

In summary, for interpreting the accelerating universe and solving the coincidence problems of cosmological constant, the holographic dark energy models are extensively studied from the different points of view. In holographic cosmology, considering that taking the natural Hubble horizon as the IR cut-off to obtain an accelerated universe is interesting, Ref. [6] presents a new generalized holographic dark energy model. In physics, this generalized model investigate a new idea to interpret the accelerating universe by using the holographic principle with including the Hubble horizon as an IR cut-off. In addition, the holographic and Ricci dark energy can be compared in the generalized model according to the new introduced parameter  $\epsilon$ . In this paper, the flat and the non-flat generalized holographic dark energy are constrained according to the current observed data. The stringent constraints on model parameters are given from the MCMC calculation. Considering the cosmic constraint on the parameter  $\epsilon$ , it is obtained that the cosmic data favor a generalized dark energy model which is more Ricci-like, since one has the relation  $\rho_{GH} = \epsilon\rho_R + (1 - \epsilon)\rho_H$  and the best fit value of parameter  $\epsilon = 1.849$  for a non-flat universe constrained from the observational data. And according to the constraint results, it is shown that relative to the Ricci dark energy model ( $\Omega_{0m} = 0.300_{-0.037-0.042}^{+0.037+0.043}$  [31]), it has a smaller value of the dimensionless matter density  $\Omega_{0m} = 0.280_{-0.032-0.040}^{+0.036+0.047}$  for the non-flat universe, which result is more consistent with the current observations and cosmological constant model [32]. In addition, based on

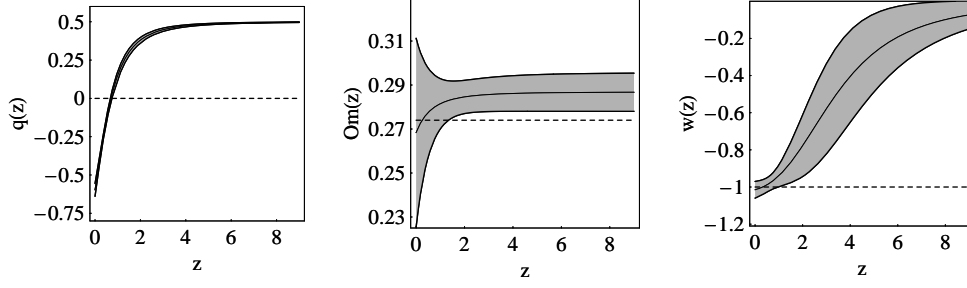


FIG. 4: The evolution of  $q(z)$ ,  $Om(z)$  and  $w_{de}(z)$  for flat generalized holographic model.

the calculation of covariance matrix the best fit evolutions of cosmological quantities such as deceleration parameter,  $Om$  parameter and EOS of generalized holographic dark energy with their confidence region are discussed. It is found that the EOS for this dark energy model can cross over the boundary of cosmological constant ( $w_\Lambda = -1$ ). And the values of transition redshift, current deceleration parameter, EOS of GH dark energy are obtained, respectively. It can be seen that for the flat universe the best fit value of  $w_{0GH} = -1.015^{+0.045}_{-0.045}$  is near to the cosmological constant model.

**Acknowledgments** The research work is supported by the National Natural Science Foundation (Grant No. 10875056) and NSF (10703001) of P.R. China.

#### Appendix A: cosmological combined constraints on generalized Ricci DE model by using MCMC method

Considering Ref. [6], another extended form dubbed as generalized Ricci dark energy is expressed,

$$\rho_{GH} = 3c^2 M_p^2 \left[1 - \eta \left(1 - \frac{H^2}{R}\right)\right] R, \quad (\text{A1})$$

where  $\eta$  is a parameter. It is easy to see when  $\eta = 1$  or  $\eta = 0$ , this generalized form reduces to Ricci or holographic dark energy, respectively. And the Friedmann equation is described for this generalized model as,

$$H^2 = H_0^2 \left[ \left(1 - \frac{2(\Omega_{0m} + \Omega_r + \Omega_k)}{2 - c^2(1 + \eta)}\right) (1 + z)^{\frac{2}{c^2(\eta-1)} + \frac{2(\eta-2)}{\eta-1}} + \frac{2(\Omega_{0m}(1+z)^3 + \Omega_r(1+z)^4 + \Omega_k(1+z)^2)}{2 - c^2(1 + \eta)} \right]. \quad (\text{A2})$$

From above equations one can see that two generalized dark energy models are equivalent when  $\epsilon = 1 - \eta$ . Figs. 5 shows the  $1D$  distributions of model parameters. And the MCMC calculation results for the non-flat universe are,  $\Omega_k = -0.0008^{+0.0089+0.0128}_{-0.0127-0.0143}$ ,  $c = 0.585^{+0.024+0.029}_{-0.045-0.049}$ ,  $\eta = -0.855^{+0.374+0.470}_{-0.366-0.448}$ , and  $\Omega_{0m} = 0.280^{+0.037+0.050}_{-0.032-0.036}$  for the best fit values.

---

[1] A.G. Riess *et al*, 1998 *Astron. J.* **116** 1009 [arXiv:astro-ph/9805201]

S. Perlmutter *et al*, 1999 *Astrophys. J.* **517** 565.

[2] B. Ratra and P.J.E. Peebles, 1988 *Phys. Rev. D.* **37** 3406

R.R. Caldwell, M. Kamionkowski and N. N. Weinberg, 2003 *Phys. Rev. Lett.* **91** 071301 [arXiv:astro-ph/0302506]

B. Feng, X.L. Wang and X.M. Zhang, 2005 *Phys. Lett. B* **607** 35 [arXiv:astro-ph/0404224]

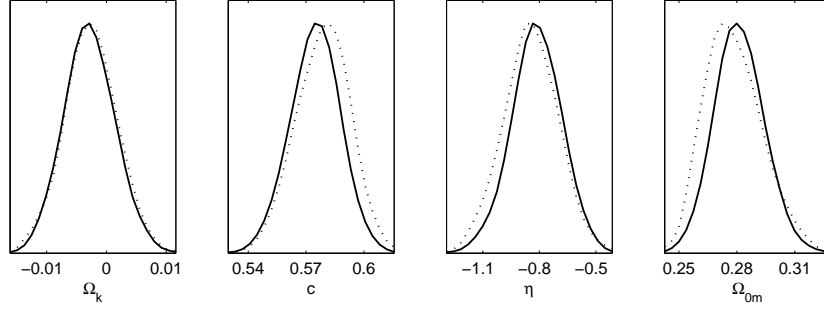


FIG. 5: The 1-D distribution of model parameters in the non-flat GR model. Solid lines are mean likelihoods of samples, and dotted lines are marginalized probabilities for 1D distribution.

J.B. Lu, E.N. Saridakis, M.R. Setare and L.X. Xu, JCAP, 2010, 03: 031 [arXiv:astro-ph/0912.0923]

J.B. Lu, L.X. Xu, and M.L. Liu, Phys. Lett. B 699 (2011) 246-250

G.P. Singh, and A.Y. Kale, Eur. Phys. J. Plus (2011) 126:83

M. Jamil, I. Hussain, and D. Momeni, Eur. Phys. J. Plus (2011) 126:80

J.B. Lu et al., Gen. Relativ. Gravit. 43, 819 (2011)

J.B. Lu et al., Eur. Phys. J. Plus (2011) 126: 92

Y.T. Wang and L.X. Xu, Phys. Rev. D 81 083523 (2010) arXiv:1004.3340

A.Y. Kamenshchik, U. Moschella and V. Pasquier, 2001 *Phys. Lett. B* **511** 265 [arXiv:gr-qc/0103004]

B.C. Paul, P. Thakur, and A. Saha, [arXiv:gr-qc/0707.4625]

J.B. Lu, Y.B. Wu, L.X. Xu, and Y.T. Wang, Chin. Phys. B 20, 079801 (2011).

[3] S.D.H. Su, Phys.Lett.B, 594, 13 (2004) [arXiv:hep-th/0403052]

M. Li, 2004 *Phys. Lett. B* **603** 1 [arXiv:hep-th/0403127]

[4] C. Gao, F. Wu, X. Chen, Y.G. Shen, Phys. Rev. D 79 043511(2009) [arXiv:0712.1394].

[5] R. G. Cai, B. Hu and Y. Zhang, [arXiv:0812.4504].

[6] L.X Xu, J.B Lu, and W.B. Li, Eur. Phys. J. C (2009) 64: 89-95

[7] V. Sahni, A. Shafieloo and A. A. Starobinsky, 2008 Phys. Rev. D 78 103502 [arXiv:astro-ph/0807.3548]

[8] R. Amanullah et al. [Supernova Cosmology Project Collaboration], [arXiv:astro-ph/1004.1711]

The numerical data of the full sample are available at <http://supernova.lbl.gov/Union>.

[9] H. Wei, arXiv:1004.4951.

[10] J. Simon, L. Verde and R. Jimenez, Phys. Rev. D **71** 123001 (2005)

[11] S.W. Allen, D.A. Rapetti, R.W. Schmidt, et al, Mon.Not.Roy.Astron.Soc. **383** 879 (2008).

[12] W.J. Percival *et al.*, [arXiv:astro-ph/0907.1660].

[13] E. Komatsu et al., [arXiv:astro-ph/1001.4538].

[14] E. Garcia-Berro, E. Gaztanaga, J. Isern, O. Benvenuto and L. Althaus, arXiv:astro-ph/9907440

A. Riazuelo, J. Uzan, Phys.Rev. D **66** 023525 (2002)

V. Acquaviva, L. Verde, JCAP **0712** 001 (2007).

[15] R.Gannouji, D. Polarski, JCAP **0805**, 018 (2008).

[16] S. Nesseris and L. Perivolaropoulos, Phys. Rev. D **72**, 123519 (2005)

L. Perivolaropoulos, Phys. Rev. D **71**, 063503 (2005)

E. Di Pietro and J. F. Claeskens, Mon. Not. Roy. Astron. Soc. **341**, 1299 (2003)

A. C. C. Guimaraes, J. V. Cunha and J. A. S. Lima, JCAP **0910**, 010 (2009)

- J.B. Lu, *Phys. Lett. B* **680**, 404 (2009)
- M. Szydlowski and W. Godlowski, 2006 *Phys. Lett. B* **633** 427
- S. Nesseris and L. Perivolaropoulos, 2007 *JCAP* **0702** 025
- U. Alam and V. Sahni, 2006 *Phys.Rev.D* **73** 084024.
- [17] N. Liang, W. K. Xiao, Y. Liu and S. N. Zhang, *Astrophys. J.* 685, 354 (2008)
- [18] L. Amati et al., *Astron. Astrophys.* 390 81 (2002).
- [19] Z.L. Yi and T.J. Zhang, 2007 *Mod. Phys. Lett. A* **22** 41-53.
- [20] R. Jimenez, L. Verde, T. Treu and D. Stern, *Astrophys. J.* **593** 622 (2003).
- [21] D. Stern, R. Jimenez, L. Verde, M. Kamionkowski and S. A. Stanford, [arXiv:astro-ph/0907.3149]  
J. Simon et al, 2005 *Phys. Rev. D* 71, 123001.
- [22] A. G. Riess *et al.*, [arXiv:0905.0695].
- [23] E. Gaztanñaga, A. Cabré and L. Hui, [arXiv:0807.3551].
- [24] R. Lazkoz and E. Majerotto, 2007 *JCAP* **0707** 015  
J.B. Lu, L.X. Xu, M.L. Liu and Y.X. Gui, 2008 *Eur. Phys. J. C* **58** 311  
L. Samushia and B. Ratra, 2006 *Astrophys. J.* **650** L5  
R. Jimenez, L. Verde, T. Treu and D. Stern, 2003 *Astrophys. J.* **593** 622.
- [25] S. Nesseris and L. Perivolaropoulos, *JCAP* **0701** 018 (2007).
- [26] D. J. Eisenstein *et al.*, *Astrophys. J.* **633** 560 (2005); W. J. Percival *et al.*, *Mon. Not. Roy. Astron. Soc.* **381** 1053 (2007)  
J.B. Lu and L.X. Xu, 2010 *Modern Physics Letters A* **25** 737-747.
- [27] A. Lewis and S. Bridle, *Phys. Rev. D* **66** 103511 (2002); URL: <http://cosmologist.info/cosmomc/>.
- [28] URL: <http://www.stanford.edu/~drapetti/fgas-module/>
- [29] D. Rapetti, S. W. Allen and J. Weller, *Mon. Not. Roy. Astron. Soc.* **360** 555 (2005).
- [30] L. Xu, W. Li, J. Lu, [arXiv:0810.4730]  
X.Zhang, [arXiv:0901.2262].
- [31] L. Xu, Y. Wang, *JCAP*,06(2010),002,[arXiv:1006.0296].
- [32] E. Komatsu et al., *Astrophys. J. Suppl.* 180, 330 (2009) [arXiv:0803.0547].